AIAA-92-2087-CP

DYNAMICS OF SPACECRAFT WITH DEPLOYING FLEXIBLE APPENDAGES

Janice D. Downer*
Department of Engineering Mechanics
University of Wisconsin, Madison, WI

K. C. Park**
Center for Space Structures and Controls
Department of Aerospace Engineering Sciences
University of Colorado, Boulder, CO

Abstract

A computational formulation for the dynamic analysis of spacecraft with deploying appendages is presented. The appendage model is based on a geometrically nonlinear beam formulation which accurately accounts for large rotational and large deformational motions. A moving finite element reference grid is incorporated within the nonlinear beam formulation to model the deployment motion. Hamilton's Law is used to formulate the general equations of motion, and a transient integration solution procedure is derived from a space-time finite element discretization of the Hamiltonian variational statement. Computational results of the methodology are presented for a classical gravity gradient stabilized satellite configuration.

1.0 Introduction

The dynamics of beam-like structures being extended from a rotating base is becoming increasingly important for the analysis of spacecraft and large space structures which deploy flexible appendages such as antennae, stabilizing booms, solar arrays, and long truss-like structures. Modern space vehicles compactly store such lightweight structures during launch, and deploy the beam-like appendages during the attitude acquisition phase or the orbit phase of the satellite. As the relatively long appendages tend to be deployed with relatively small extension rates, the transient effect of deployment may be felt over a long period of time. Due to the highly flexible nature of these appendages, potentially large deformations may occur during typical spacecraft operations during and after the deployment phase. To study the effect of the deployment of highly flexible appendages on the attitude dynamics of an orbiting satellite, the objective of this paper is to develop a general computational formulation of the dynamics of axially moving and rotating beams.

Early works which investigated the effect of appendage deployment on the overall satellite motion modeled the appendages as point masses[1] and rigid bodies.[2,3] Flexible appendages were then considered for specific spacecraft configurations[4,5], and a general formulation for flexible satellite dynamics with deploying appendages are presented in Refs. 6-8. In these initial flexible analyses, the displacement of a flexible member is modeled by a linear combination of space-dependent admissible functions weighted by time-dependent generalized coordinates. Alternative approaches which move beyond this limiting assumption of small elastic deformations have been presented in recent works. In Ref. 9, the appendage is modeled as a series of elastically connected rigid links, and the links outside the rigid body at a given time are considered when deriving equations of motion. In Ref. 10, a continuum-based formulation of the constant velocity extrusion of a nonlinear elastica from a fixed horizontal guide is developed for planar motion. A finite element formulation of this same problem based on a geometrically nonlinear beam model was presented by the present authors in Ref. 11. To the best of our knowledge, there exist no general modeling and analysis capability for axially moving beams of variable cross-sections that are subject to large three-dimensional motions. To provide such a capability, the present paper extends the methods of Ref. 11 to model the fully three-dimensional rotations and possible large deformations of beam-type structures which deploy from a rotating and orbiting central body.

The following approach has been adopted in the present work to model the fully three-dimensional motion of orbiting satellites with deploying beam-like appendages. First, the appendage model is based on a geometrically exact beam theory. As substantiated in recent literature[12-20], such a theory accurately models both large rotational and large deformational beam motion, and significantly advances the modeling capabilities achievable by standard assumed mode representations of beam flexibility. In the present work, the nonlinear beam formulation of Refs. 18-20 is readily extended to model the dynamics of deployment by introducing a moving rigid reference for the kinematic variables which is extending from an initial satellite orientation with a prescribed deployment speed. In the finite element discretization of this moving beam formulation, a variable grid approach is employed such that the number of discrete points are fixed and the length of each discrete beam element is allowed to vary. From the moving reference kinematic description, Hamilton's Law is used to formulate the equations of motion. The use of Hamilton's Law simplifies the numerical treatment of complex convective accelerations which are a result of the moving reference model. In addition, Hamilton's Law provides a physical variational basis for a space-time finite element discretization which leads to an attractive step-by-step implicit integration algorithm.[21-25] Within the present work, the Hamiltonian variational formulation and finite element evaluation is successfully extended to include finite rotation and deployment modeling capabilities. A specific application of the general methodology to a gravity gradient

* Assistant Professor, Member AIAA

** Professor, Assoc. Fellow AIAA

satellite configuration in an arbitrary orbit is considered.

To this end, the rest of the paper is organized as follows. Section 2 presents the kinematics of the beam deployment. The formulation of the equations of motion from Hamilton's Law is presented in Section 3. The space-time finite element discretization of the Hamiltonian formulation is presented in Section 4. Section 5 then presents results of the satellite librational and vibrational response of a classical gravity gradient stabilized system during and after deployment of flexible beam-like appendages.

2.0 Beam Kinematics

An accurate representation of finite rotational and finite deformational behavior of a beam-like structure can be achieved through the use of a nonlinear, geometrically exact beam theory. This so-called geometrically exact theory for the large overall motion of an elastic continua was originally used by Simo[12] to describe the dynamics of flexible beam-like structures undergoing both finite rotations and finite deformations, and an elegant rederivation of the theory was recently presented by Hodges.[15] As substantiated in this and other recent literature, significant advantages and improvements can be obtained by employing geometrically exact theories to model structures undergoing large overall motions.[12–20] In contrast to the conventional modeling techniques which distinguish the elastic deformations from the rigid body displacements, the new theories express the rigid body motions and the elastic deformations together by referencing all motion directly to an inertially fixed frame. As the kinematic variables thus implicitly contain information of both rigid motion and deformations without distinction, finite strain definitions which are invariant to large rigid body motions are then used when defining the internal force of an elastically deformed and rotated component. Along with their inherent objectivity to rigid body motions, such finite strain definitions model coupled extensional, flexural, torsional, and transverse shear deformations. In addition, any motion induced stiffness such as the centrifugal stiffness which is experienced during a high speed rotation of a flexible member is also automatically accounted for by the finite strain definitions. The objective of this paper is to incorporate such a theory when modeling the dynamics of deployment of highly flexible beam-like structures.

In the geometrically exact theory, the total displacements of the combined elastic and rigid motion are strategically treated as the unknowns from the onset. To geometrically describe an arbitrarily deformed and rotated beam configuration, a space-curved line is introduced to represent the locus of material points defining the beam centroidal-axis, and a set of planar cross-sections are then associated with each material point on this axis. The beam cross-sections are assumed to be symmetric such that the beam neutral axis and centroidal-axis coincide. For the reference configuration of an undeformed beam, the line of centroids is taken to be straight and the cross-sections are oriented perpendicular to this line such that there is no initial twist of the beam. As the beam deforms, the line of centroids assumes a curved line in space and the cross-sections independently assume a new orientation. In the new orientation, the cross-section is not necessarily perpendicular to the neutral axis of the deformed beam due to effects of transverse shear and torsional deformation. Warping deformation of the cross-section is not taken into consideration in the present formulation.

An orthogonal triad of basis vectors ($\mathbf{b}_1, \mathbf{b}_2, \mathbf{b}_3$) are attached to and rotate with the cross-section at a particular material point on the neutral axis. The axes $\mathbf{b}_2$ and $\mathbf{b}_3$ lie in the plane of the cross-section and the axis $\mathbf{b}_1$ is normal to the cross-section. The origin of these basis vectors coincide with the centroid of the cross-section. As shown in Figure 1, an arbitrary material point within the deformed beam configuration can be identified by the vector

$$\mathbf{r} \;=\; \mathbf{X} + \mathbf{u} \;+\; \ell_2\,\mathbf{b}_2 \;+\; \ell_3\,\mathbf{b}_3$$

where $\mathbf{X}$ represents the position vector of a particle on the initial centroidal axis and thus the cross-section within which the material point resides; $\mathbf{u}$ is the displacement vector of a particle on the initial centroidal axis; $\mathbf{b}_2$ and $\mathbf{b}_3$ are basis vectors in the plane of the cross-section of the current body-fixed reference frame; and ℓ_2 and ℓ_3 are the respective body-fixed components of the position vector which locates the arbitrary material point relative to the centroidal point of the particular cross-section. This is rewritten in a compact component form as

$$\mathbf{r} \;=\; \{\, X \;+\; u \,\}^T\,\mathbf{e} \;+\; \ell^T\,\mathbf{b} \qquad (2.1)$$

where the notation $\mathbf{e} = \{\mathbf{e_1}, \mathbf{e_2}, \mathbf{e_3}\}^T$ represents the basis vectors of the inertial reference frame; $\mathbf{b} = \{\mathbf{b_1}, \mathbf{b_2}, \mathbf{b_3}\}^T$ represents the basis vectors of the body-fixed reference frame attached to the beam cross section; $X^T = \{X_1, X_2, X_3\}$ represents the inertial components of the reference neutral axis position; $u^T = \{u_1, u_2, u_3\}$ represents the inertial components of the neutral axis displacement, and $\ell^T = \{0, \ell_2, \ell_3\}$ represents the body-fixed components of the distance from the beam neutral-axis to the material point located on the beam cross-section. An orthogonal transformation matrix R is

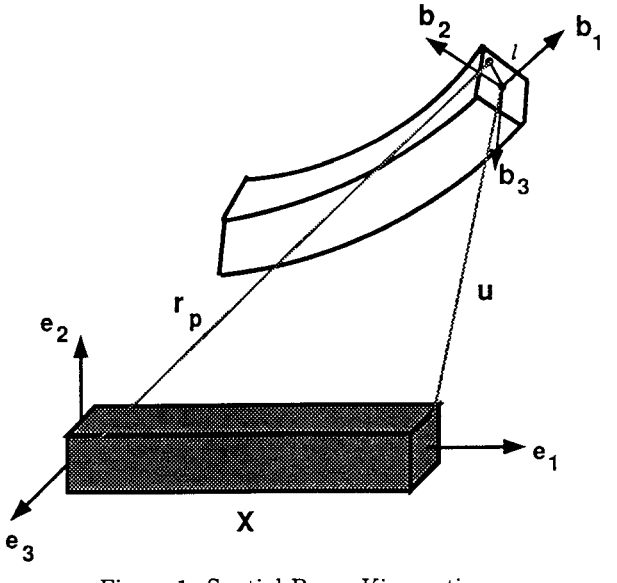

Figure 1: Spatial Beam Kinematics

introduced to describe the orientation of the so-called body fixed reference frame with respect to an inertially fixed reference frame such that $\mathbf{b}_i = R_{ij}\,\mathbf{e}_j$. The degrees of freedom of the beam model are thus a set of translational coordinates representing the dispacement of the neutral axis u and a set of finite rotational coordinates which parameterize the cross-section orientation transformation matrix R.

This type of kinematic description does not distinguish between displacements arising from rigid body motion and those due to elastic deformation. As such, finite deformation theories which are naturally invariant to any rigid motions contained within the kinematic variables are necessary for this type of formulation. The most common approach to a finite deformation analysis is based on a Lagrangian description in which all stresses and strains are measured with respect to the original, undeformed configuration of the beam.[12-17] A Piola-Kirchhoff stress representation is used within the analysis in which the traction forces acting on a deformed surface element are referenced back to the undeformed configuration. A generalized Hooke's law modeling hyperelastic constitutive behavior is then employed to relate the Piola-Kirchhoff stresses to a Lagrangian strain definition which is based on a direct comparison of the current shape of the continuum back to its original reference configuration. The Lagrangian strain definitions are invariant to all rigid body motion contained within the beam kinematic variables $\mathbf{u}$ and R, and they directly model coupled extensional, flexural, torsional, and transverse shear deformations.

While the Lagrangian formulations referenced above are mathematically sound, the stresses transmitted in the deformed state are referred to the initial state in a way that is physically artificial. An Eulerian formulation incorporates a physically natural reference of the current deformed beam configuration for the stress and strain descriptions. In the present formulation the stresses and strains resulting from beam deformation are computed with respect to a *convected* reference frame.[18-20] The introduction of this convected frame decomposition of the Cauchy stress representation leads to a deformation description which has physical meaning as the convected strain components computed within the present formulation coincide with physical strains measured by sensors located and operating on the deformed structure. This particular formulation is thus highly conducive to future applications which will involve active control of the deployment motion of a highly flexible beam-like structure.

The basis vectors of the convected reference frame $\{\mathbf{a}_1, \mathbf{a}_2, \mathbf{a}_3\}$ shown in Figure 2 are defined such that $\mathbf{a}_1$ is tangent to the neutral axis of the deformed beam.[18-20] Given this tangent $\mathbf{a}_1$, the $\mathbf{a}_2$ vector is defined as the cross product of $\mathbf{a}_1$ with the $\mathbf{b}_3$ axis of the body-fixed reference frame, and the remaining axis $\mathbf{a}_3$ is defined to complete the right-hand coordinate system. This particular construction of the $\mathbf{a}$ reference frame is an approximation applicable for moderate strains such that the relative difference between the convected reference frame and the body-fixed reference frame attached to the beam cross-section provides a measure of the transverse shear and torsional deformations. The orthogonal transformation matrix T is introduced to describe the orientation of the convected reference frame with respect to the inertial reference frame such that $\mathbf{a}_i = T_{ij}\,\mathbf{e}_j$. The formulation and computational implementation of this convected coordinate Cauchy formulation of the large deformation/large rotation dynamics of highly flexible beam-like structures is detailed in Refs. 18-20.

This geometrically exact, convected coordinate beam theory is extended to model the deployment of a beam-like structure from a rotating and orbiting base as follows. To include the effect of deployment within the general kinematic description (2.1), the undeformed beam configuration X is now defined as a function of time $\bar{X}(t)$. The displacement variables locating the position of the deformed neutral axis are measured from a set of material particles which represent the position of a phantom beam rigidly extending in a fixed direction with a prescribed velocity. As such, the position vector $\mathbf{r}$ which locates an arbitrary point within the changing spatial configuration occupied by the beam in reference to a particular moving material point is now described as

$$\mathbf{r} = \{\, \bar{X}(t) + u \,\}^T \mathbf{e} + \ell^T \mathbf{b} \qquad (2.2)$$

where $\bar{X}(t)$ represents time-dependent inertial coordinates of the rigid phantom beam neutral axis. To account for the orbit trajectory, a position vector $\mathbf{Z}$ can be introduced as shown in Figure 3 to locate the center of mass of the satellite such that

$$\mathbf{r} = \{\, Z + \bar{X}(t) + u \,\}^T \mathbf{e} + \ell^T \mathbf{b} \;. \qquad (2.3)$$

For this particular application, the origin of the phantom beam coordinates will coincide with the location of the satellite center of mass relative to the earth, and the neutral axis displacements $\mathbf{u}$ will be measured from a phantom beam which is translating (but not rotating) in orbit with the satellite center of mass. The location of the center of

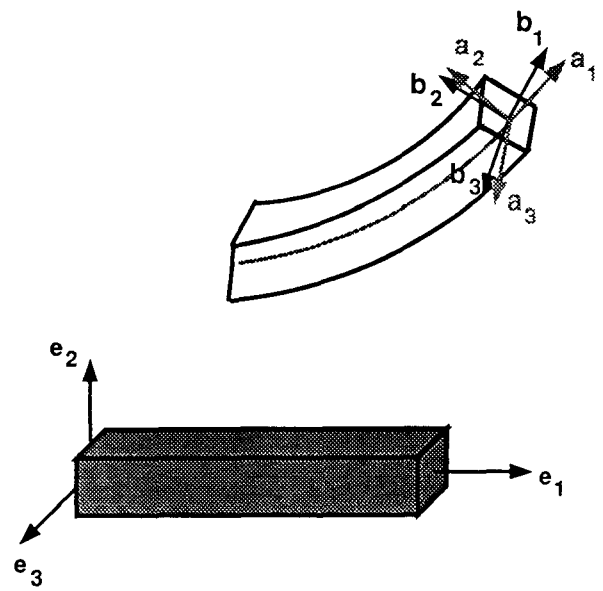

Figure 2: Convected Reference Frame

mass of a satellite in orbit is governed by the differential equation

$$\ddot{\mathbf{Z}} = -\frac{\mu \mathbf{Z}}{\|\mathbf{Z}\|^3} \tag{2.4}$$

where μ is the gravitational constant, and a solution of this motion can readily be obtained. It will be assumed in the present analysis that the center of mass of a deformed beam remains in a very small neighborhood of the center of mass of the rigid phantom beam such that $\mathbf{Z}$ will coincide with the origin of the phantom beam. This type of decomposition was utilized in Ref. 27 to get a realistic numerical solution for the structural deformations as $\| \bar{\mathbf{X}} + \mathbf{u} \| \ll \| \mathbf{Z} \|$.

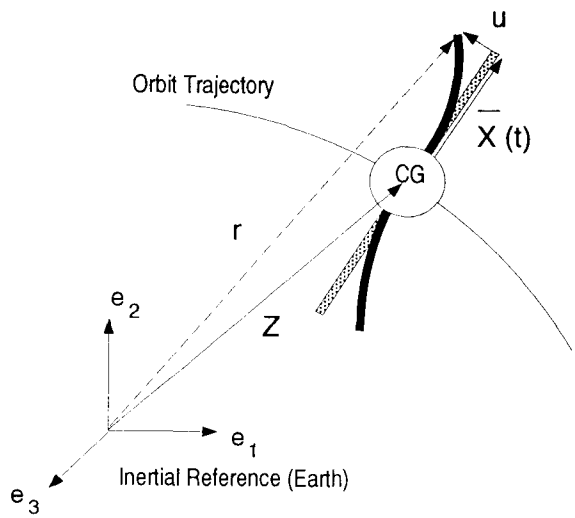

Figure 3: Orbit Kinematics

The discrete interpretation of inertial coordinates of the rigid phantom beam is given as follows. A variable finite element grid shown in Figure 4 is employed in which a fixed number of moving reference nodes are defined to represent the changing length of a phantom beam rigidly extending in a fixed directed with a given deployment velocity. The location of these moving reference nodes $\bar{X}_i(t)$ are determined by spatially dividing the total current length of the rigid phantom beam with an equal number of elements, and then projecting these nodes along a given fixed axis $\mathbf{d}_1$ representing the initial direction of the deployment. In the present analysis, it will be assumed that the deployment velocity will remain constant or be piecewise constant. If the prescribed deployment speed is a constant value of V, the total length of the rigid phantom beam at time t is $V\,t$. The inertial coordinates of the position of a particular reference node i are given as

$$\bar{X}_i\,(t) = \frac{(\,i\,-\,1\,)\,V\,t}{n_{ele}} \begin{Bmatrix} \mathbf{d}_1 \cdot \mathbf{e}_1 \\ \mathbf{d}_1 \cdot \mathbf{e}_2 \\ \mathbf{d}_1 \cdot \mathbf{e}_3 \end{Bmatrix} \tag{2.5}$$

where n_{ele} represents the fixed number of variable size elements and $\mathbf{d}_1 \cdot \mathbf{e}_j$, $j = 1,3$ represents the direction cosines which orient the initial deployment direction with respect to the inertial reference frame. The degrees of freedom of the beam finite element model, namely the nodal displacement coordinates $\mathbf{u}_i$ of the beam neutral axis and the nodal rotational coordinates R_i of the cross-section orientation, are now referred to an appropriate moving nodal coordinate of the rigid phantom beam. It is noted that only the length of the rigid phantom beam is changing, and that its orientation remains fixed in the initial deployment direction. The ensuing rotations of the actual deformed beam configuration which result from initial conditions and external forces are automatically accounted for within the geometrically exact beam model, and there is no need to rotate the rigid phantom beam. This so-called variable grid approach, where the number of finite element nodes remains fixed and the length of each beam element is allowed to vary, has been chosen as the data structure, computer implementation, and geometric interpretation is much more straightforward than an alternative approach which would employ a growing number of finite elements of fixed size.

To complete the kinematic description of the present beam model, the velocity and acceleration of a material particle within the axially extending beam is given as follows. Since the Eulerian based kinematic description (2.2) measures the displacement variables from a moving reference, the velocity of a material particle is defined as

$$\mathbf{v}_i = \frac{D}{Dt}\,\mathbf{r}_i \quad , \qquad \frac{D}{Dt} \equiv \frac{\partial}{\partial t} + \frac{d\,\bar{X}_i}{dt}\,\frac{\partial}{\partial \bar{X}_i} \tag{2.6}$$

where $d\bar{X}_i/dt$ is easily obtained from (2.5). The moving node formulation necessitates the inclusion of convective rate of change of the variable in addition to the local rate of change of the variable with respect to time. In order to both simplify the convective velocity term and be consistent with the present beam formulation which is based on convected

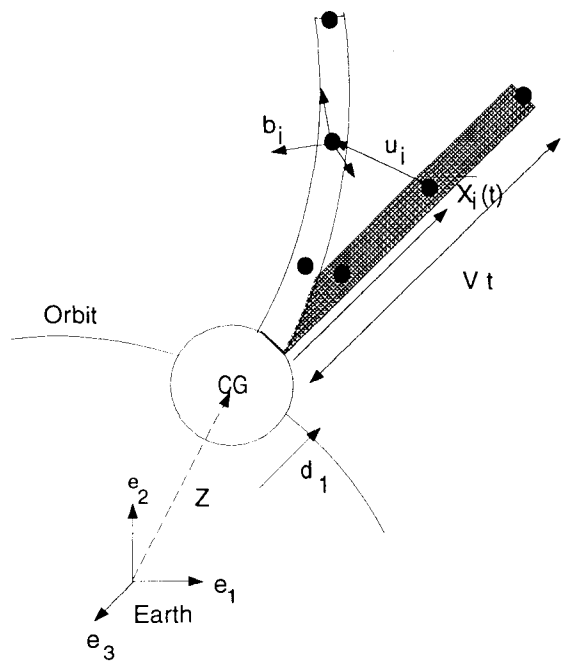

Figure 4: Deployment Kinematics

coordinate stress and strain definitions, the material time derivative will be expressed in terms of convected spatial coordinates ζ_i as opposed to the inertial coordinates $\bar{X}_i$ as

$$\frac{D}{Dt} = \frac{\partial}{\partial t} + v_i^a \frac{\partial}{\partial \zeta_i} \quad , \qquad v_i^a \equiv T_{ij} \frac{d\bar{X}_j}{dt} \quad . \tag{2.7}$$

Now, the nodal displacements $\mathbf{u}$ locating the deformed neutral axis are solely a function of the $\mathbf{a}_1$ convected coordinate which is tangent to the deformed neutral axis $\xi \equiv \zeta_1$. Likewise, as the plane of the cross-section strictly rotates without any warping deformation, the nodal orientations R are also solely a function of the convected tangent coordinate ξ. As such, the following simplified material time derivative

$$\frac{D}{Dt} = \frac{\partial}{\partial t} + V^a \frac{\partial}{\partial \xi} \quad , \qquad V^a = T_{1j} \frac{d\bar{X}_j}{dt} \quad . \tag{2.8}$$

can be used in conjunction with the present beam kinematic variables.

The velocity and acceleration of a material particle can now be derived by applying (2.8) to the Eulerian description (2.2). For the body-fixed coordinates ℓ which remain fixed with respect to the $\mathbf{b}$-basis attached to the cross-section, the appropriate definitions to be employed to account for the rotating reference are given as

$$\frac{\partial}{\partial t} = \frac{\partial^b}{\partial t} + \tilde{\omega} \quad , \qquad \tilde{\omega} = -\frac{\partial R}{\partial t} R^T \tag{2.9}$$

$$\frac{\partial}{\partial \xi} = \frac{\partial^b}{\partial \xi} + \tilde{\kappa} \quad , \qquad \tilde{\kappa} = -\frac{\partial R}{\partial \xi} R^T \tag{2.10}$$

where the superscript b represents the derivatives with respect to the $\mathbf{b}$ frame, and $\tilde{\omega}$ and $\tilde{\kappa}$ are the angular velocity and curvature tensors of the $\mathbf{b}$ frame, respectively. Application of (2.8), (2.9), and (2.10) to (2.2) gives the following expressions for the velocity and acceleration of a material particle as

$$\frac{D\,\mathbf{r}}{Dt} = \mathbf{e}^T \left[\left(\dot{\bar{X}} + \dot{u} \right) + V^a \frac{\partial^e u}{\partial \xi} \right] + \mathbf{b}^T \left[\tilde{\omega} + V^a \tilde{\kappa} \right] \ell \tag{2.11}$$

$$\begin{aligned} \frac{D^2\,\mathbf{r}}{Dt^2} = {} & \mathbf{e}^T \left[\frac{\partial^{e^2} u}{\partial t^2} + 2\,V^a \frac{\partial^{e^2} u}{\partial t\,\partial \xi} + V^{a^2} \frac{\partial^{e^2} u}{\partial \xi^2} \right] \\ & + \mathbf{b}^T \left[\frac{\partial^b \tilde{\omega}}{\partial t} + \tilde{\omega}\tilde{\omega} + V^a \left(\frac{\partial^b \tilde{\omega}}{\partial \xi} + \frac{\partial^b \tilde{\kappa}}{\partial t} + \tilde{\omega}\tilde{\kappa} + \tilde{\kappa}\tilde{\omega} \right) + V^{a^2} \left(\frac{\partial^b \tilde{\kappa}}{\partial \xi} + \tilde{\kappa}\tilde{\kappa} \right) \right] \ell \quad . \end{aligned} \tag{2.12}$$

3.0 Hamiltonian Equations of Motion

From this detailed description of the kinematics of axially moving beams, we move to a discussion of a suitable formulation equations of motion for this problem. A fundamental principle of mechanics suited for the application of finite element approximate solution techniques is the principle of virtual work given as

$$\int_\vartheta \delta r_i\, \rho \ddot{r}_i\, d\vartheta + \int_\vartheta \sigma_{ij}^e \frac{\partial \delta r_i}{\partial x_j}\, d\vartheta = \int_\vartheta \delta r_i f_i\, d\vartheta + \int_S \delta r_i t_i\, dS \quad . \tag{3.1}$$

In the above equation, the Cartesian coordinates x_i represent the particle position after some deformation has taken place, ϑ the volume of the deformed beam, δr_i a kinematically admissible virtual displacement, $\ddot{r}_i$ the acceleration of a material particle, f_i the external force per unit mass, and t_i the stress vector acting on a surface with outward normal components n_i. Likewise, σ_{ij}^e represents the Cartesian components of the Cauchy stress tensor, and ρ is the mass density. The principle of virtual work is widely used as a variational source to formulate a discrete set of ordinary differential equations in time using spatial finite element techniques. Standard numerical time integration techniques are then used to solve the second-order differential equations.

Such a discrete formulation will become quite complex for the particular kinematics of the beam deployment discussed in the preceding section as a result of the expression for the absolute acceleration of a material particle. As seen in (2.12), this acceleration expression now contains second-order spatial derivatives as well as coupled spatial/temporal derivatives in addition to the second-order time derivatives as a result of the moving reference for the dynamic variables. As such, higher order spatial finite element approximation functions must be employed to form the discrete equations than would have been necessary for a standard fixed reference formulation. The numerical time integration of these equations would then need to be addressed.

These complexities can be avoided if Hamilton's Law of Varying Action is used to formulate the equations of motion. Hamilton's Law is a weak or variational form in time of the principle of virtual work which transform the acceleration expressions to first-order form. From this variational statement, a finite element discretization in time can be applied simultaneously with a discretization in space to achieve a viable and simple numerical treatment of the inertia force of the deploying beam.

To derive Hamilton's Law, the integral over an arbitrary time interval of the principle of virtual work is considered such that the acceleration term can be integrated by parts to lead equation (3.1) to the form

$$\int_{t_1}^{t_2} \int_\vartheta \left\{ \rho\, \dot{r}_i\, \delta \dot{r}_i - \sigma_{ij}^e \frac{\partial \delta r_i}{\partial x_j} + \delta r_i f_i \right\} d\vartheta\, dt = \left[\int_\vartheta \rho\, \dot{r}_i \delta r_i\, d\vartheta \right] \Big|_{t_1}^{t_2} \quad . \tag{3.2}$$

For the present deployment problem, the inertia term which must be integrated by parts involves the material time derivative definition (2.8) and a spatial integration over a time dependent volume $\vartheta(t)$ as

$$\int_{t_1}^{t_2} \int_{\vartheta(t)} \rho \frac{D^2\, r_i}{Dt^2}\, \delta r_i\, d\vartheta\, dt \quad . \tag{3.3}$$

The Reynolds transport theorem can be invoked to properly interchange a time derivative and a time-dependent spatial

integral of the mass density and an arbitrary function F as[26]

$$\frac{D}{Dt}\int_{\vartheta(t)} \rho\, F\, d\vartheta \;=\; \int_{\vartheta(t)} \rho\, \frac{D\,F}{Dt}\, d\vartheta$$

such that

$$\int_{t_1}^{t_2}\int_{\vartheta(t)} \rho\, \frac{D^2 r_i}{Dt^2}\, \delta r_i\, d\vartheta\, dt \;=\; \int_{\vartheta(t)} \rho\, \frac{Dr_i}{Dt}\, \delta r_i\, d\vartheta \;\Big|_{t_1}^{t_2} - \int_{t_1}^{t_2}\int_{\vartheta(t)} \rho\, \frac{Dr_i}{Dt}\, \delta r_i\, d\vartheta\, dt \;. \tag{3.4}$$

For the particular application of a beam in orbit where the trajectory of the satellite center of mass is explicitly modeled in the kinematic description (2.3), the acceleration is given as

$$\int_{t_1}^{t_2}\int_{\vartheta(t)} \rho\, \frac{D^2 r_i}{Dt^2}\, \delta r_i\, d\vartheta\, dt \;= \; \delta F_b^I \;-\; \delta F_i^I \;+\; \int_{t_1}^{t_2}\int_{\vartheta(t)} \rho\, \ddot{Z}_i\, \delta r_i\, d\vartheta\, dt$$

where the first two terms correspond to the boundary inertia and the interior inertia that were given above in (3.4). The translational acceleration $\ddot{Z}$ of the satellite center mass which coincides with the origin of the phantom beam reference coordinates will be considered as an external inertial force acting on the beam coordinates r_i given by the kinematic description (2.2). Hamilton's Law is thus given for the present Eulerian-type formulation as

$$\int_{t_1}^{t_2}\int_{\vartheta(t)} \left\{ \rho \frac{D\, r_i}{Dt}\frac{D\delta r_i}{Dt} \;-\; \sigma_{ij}^e\, \frac{\partial \delta r_i}{\partial x_j} \;+\; (f_i \;-\; \rho \ddot{Z}_i)\, \delta r_i \right\} d\vartheta\, dt \;=\; \int_{\vartheta(t)} \rho\, \frac{D\, r_i}{Dt}\, \delta r_i\, d\vartheta \;\Big|_{t_1}^{t_2} . \tag{3.5}$$

Complete expressions for the individual terms within the above equation which incorporate the specific kinematics of the beam deployment are given as follows.

3.1 Beam Acceleration

From the kinematic description (2.2) of the beam deployment problem, the interior term of the inertia operator is given as

$$\int_{t_1}^{t_2}\int_{\vartheta(t)} \rho\, \frac{Dr_i}{Dt}\frac{D\delta r_i}{Dt}\, d\vartheta\, dt \;= \tag{3.6}$$

$$\int_{t_1}^{t_2}\int_{\xi} \left\{ \left\{ \dot{u}^T \;+\; V^a\, \frac{\partial u^T}{\partial \xi} \right\} M \left\{ \frac{\partial \delta u}{\partial t} \;+\; V^a\, \frac{\partial \delta u}{\partial \xi} \right\} + \left\{ \omega^T \;+\; V^a\, \kappa^T \right\} J \left\{ \delta\omega \;+\; V^a\, \delta\kappa \right\} \right\} d\xi\, dt \;.$$

In the above expression, M and J represent the area and inertia properties of the beam cross-section as

$$M \;=\; Diag\, \{\, m\,,\, m\,,\, m\,\}$$

$$m \;=\; \int_A \rho\, dA \quad,\quad J \;=\; \int_A \rho\, \tilde{\ell}\tilde{\ell}^T\, dA \quad,$$

$\delta\omega$ and $\delta\kappa$ represent the variation of angular velocity and curvature, respectively, defined as

$$\delta\omega \;=\; \frac{\partial \delta\alpha}{\partial t} \;+\; \tilde{\omega}\, \delta\alpha \tag{3.7}$$

$$\delta\kappa \;=\; \frac{\partial\, \delta\alpha}{\partial \xi} \;+\; \tilde{\kappa}\, \delta\alpha \quad, \tag{3.8}$$

and $\delta\alpha \;\equiv\; \{\, \delta\alpha_1, \delta\alpha_2, \delta\alpha_3 \,\}^T$ are the virtual rotations of the **b** reference frame defined as

$$\delta\tilde{\alpha} \;=\; -\,\delta R\, R^T \;=\; \begin{bmatrix} 0 & -\delta\alpha_3 & \delta\alpha_2 \\ \delta\alpha_3 & 0 & -\delta\alpha_1 \\ -\delta\alpha_2 & \delta\alpha_1 & 0 \end{bmatrix} . \tag{3.9}$$

The resulting expression for the boundary term of the inertia operator is given as

$$\left[\int_{\vartheta(t)} \rho\, \frac{D\, r_i}{Dt}\, \delta r_i\, d\vartheta \right] \Big|_{t_1}^{t_2} \;= \tag{3.10}$$

$$\left[\int_{\xi(t)} \left\{ \left\{ \dot{u}^T \;+\; V^a\, \frac{\partial u^T}{\partial \xi} \right\} M\, \delta u \;+\; \left\{ \omega^T \;+\; V^a\, \kappa^T \right\} J\, \delta\alpha \right\} d\xi \right] \Big|_{t_1}^{t_2} .$$

3.2 Beam Internal Force

The expression representing the internal force of a deformed beam

$$\delta F^S \;\equiv\; \int_{t_1}^{t_2}\int_{\vartheta} \sigma_{ij}^e\, \frac{\partial \delta r_i}{\partial x_j}\, d\vartheta\, dt \tag{3.11}$$

is evaluated as follows. As stated earlier, the present formulation retains the true Cauchy stress representation such that the current deformed beam is used as a reference for all stress and strain measurements. In order to make the present Eulerian type formulation and computational implementation more tractable, the present formulation introduces a convected reference frame within the deformed beam configuration. This reference frame is defined such that one basis vector $\mathbf{a}_1$ lies tangent to the deformed neutral axis. The internal force of a beam member is then expressed in terms of the convected frame stress tensor components σ_{ij}^a, the convected frame spatial coordinates ξ_i, and the convected frame rotational tensor T_{ij} as

$$\int_{\vartheta} \sigma_{ij}^e\, \frac{\partial \delta r_i}{\partial x_j}\, d\vartheta \;=\; \int_{\vartheta} T_{mi}\, \frac{\partial \delta r_i}{\partial \zeta_k}\, \sigma_{mk}^a\, d\vartheta \quad . \tag{3.12}$$

This general expression is tailored to the present beam kinematic description as

$$\int_{\vartheta} T_{mi}\, \frac{\partial \delta r_i}{\partial \zeta_k}\, \sigma_{mk}^a\, dV \;= \tag{3.13}$$

$$\int_{\xi} \{\, \delta\gamma^T\, N_\gamma \;+\; \delta\kappa^T\, M_\kappa \,\}\, d\xi$$

where $\delta\gamma$ represents the membrane and two transverse shear strains, $\delta\kappa$ represents the torsion and two bending strains; N_γ and M_κ represents the conjugate resultant stress forces and moments per unit length, respectively, and

ξ is the convected coordinate tangent to the beam neutral axis. The virtual strain definitions are derived in Ref. 18 as

$$\delta\gamma \;=\; \mathbf{T}\,\frac{\partial \delta u}{\partial \xi} \;+\; \left\{ \begin{array}{c} 0 \\ -\delta\beta_3 \\ \delta\beta_2 \end{array} \right\} \;, \quad \delta\kappa \;=\; \frac{\partial\, \delta\beta}{\partial \xi} \tag{3.14}$$

where $\delta\beta \;=\; S^T\,\delta\alpha$ are the virtual rotations of the cross-section referred to the convected frame and S is the transformation matrix between the body-fixed basis vectors attached to the cross-section $\mathbf{b}$ and the convected basis vectors $\mathbf{a}$ such that $\mathbf{b}_i \;=\; S_{ij}\,\mathbf{a}_j$. From (3.14), we can write the strain-displacement operator as

$$[\; B \;] \;=\; \left[\begin{array}{cc} \mathbf{T}\frac{\partial^a}{\partial \xi} & \tilde{i}_1\; S^T \\ \mathbf{0} & S^T(\;\tilde{\kappa}_S \;+\; I\;\frac{\partial^b}{\partial \xi}\;) \end{array} \right] \tag{3.15}$$

where $\tilde{i}_1$ is the skew-symmetric matrix formed from the components $i_1 = (1,0,0)$, and $\tilde{\kappa}_S^T$ is the curvature tensor of the beam denoting the spatial rate of change of the body-fixed reference frame as seen with respect to the convected coordinate system given as

$$\tilde{\kappa}_S^T \;=\; \frac{\partial^a S}{\partial \xi}\, S^T \quad , \qquad S \;=\; R\,T^T \quad .$$

From this overview, the virtual work of the internal force is thus given as

$$\int_{t_1}^{t_2} \int_{\vartheta} \sigma_{ij}^e\, \frac{\partial \delta r_i}{\partial x_j}\; d\vartheta\; dt \;\; = \tag{3.16}$$
$$\int_{t_1}^{t_2} \int_{\xi(t)} \{\; \delta u^T\; \delta\alpha^T \;\}\; [\; B \;]^T \; \left\{ \begin{array}{c} N_\gamma \\ M_\kappa \end{array} \right\}\; d\xi\; dt \quad .$$

The constitutive laws used within the present formalism to deduce N_γ and M_κ are given as follows. When a Cauchy stress representation is employed for a finite deformation/rotation problem, it is necessary to use constitutive equations which relate an objective stress-rate tensor, such as the Truesdell or the Jaumann stress rate tensors, to an energetically conjugate strain rate tensor. A convected coordinate decomposition of the Truesdell constitutive law leads to the following resultant stress-strain relations

$$\dot{N}_\gamma \;=\; C_\gamma\,\dot{\gamma} \quad , \quad \dot{M}_\kappa \;=\; C_\kappa\,\dot{\kappa} \tag{3.17}$$

where the constitutive matrices are given as

$$C_\Gamma \;=\; Diag\;[\; EA, GA_2, GA_3 \;] \tag{3.18}$$
$$C_K \;=\; Diag\;[\; GJ, EI_2, EI_3 \;] \tag{3.19}$$

and EA is the axial stiffness, GA_2 and GA_3 are the shear stiffnesses along $\mathbf{b}_2$ and $\mathbf{b}_3$; GJ is the torsional stiffness; EI_2 and EI_3 are the bending stiffnesses relative to $\mathbf{b}_2$ and $\mathbf{b}_3$. The energetically conjugate strain rate definitions introduced in (3.17) are of the same differential operator form as virtual strain definitions given in (3.14). The numerical implementation of the above elastic constitutive law is straightforward as a result of the convected coordinate decomposition; the beam resultant stresses at time t^{n+1} are obtained from the stresses at time t^n via the following additive stress update procedure

$$N^{n+1} \;=\; N^n \;+\; C_\gamma\,\Delta\gamma \tag{3.20}$$
$$M^{n+1} \;=\; M^n \;+\; C_\kappa\,\Delta\kappa \tag{3.21}$$

where $\Delta\gamma$ and $\Delta\kappa$ are incremental strains numerically deduced from the corresponding rate definitions in a manner that is computationally invariant to any large rigid motions contained within the kinematic variables. Further details of the formulation and computational implementation of this convected coordinate Cauchy formulation of the large deformation/large rotation dynamics of highly flexible beam-like structures are given in Refs 18-20.

3.3 External Gravitational Force

The external force acting on an orbiting beam due to the gravitational field of the earth is given as follows. The gravitational force acting on a material point of mass ρA located at a distance $\|\mathbf{z}\|$ from the earth is given as

$$f_g \;=\; -\frac{\mu\;\rho A\;z}{\|\mathbf{z}\|^3} \tag{3.22}$$

where μ is the gravitational constant and $\mathbf{z}$ is the total position vector of the point mass from the inertial origin of the center of mass of the earth. A reasonable assumption for the application of this expression to the present beam model is that the beam mass is concentrated along the line of centroids. The position vector from the earth center of mass to a particle on the line of centroids can be decomposed as

$$\mathbf{z} \;=\; \mathbf{Z} \;+\; \mathbf{x} \tag{3.23}$$

where $\mathbf{Z}$ is locates the center of mass of the beam from the earth and $\mathbf{x}$ then locates the line of centroids from the beam center of mass. This type of decomposition was introduced in the kinematic description (2.3) such that the origin of the rigid phantom beam translates in orbit with the satellite center of mass. In this formulation, the acceleration of Z is considered as a known external inertia force such that the external force acting on the beam coordinates $\mathbf{x} \;\equiv\; \bar{\mathbf{X}} \;+\; \mathbf{u}$ due to the gravitational field is given as

$$\int_{t_1}^{t_2} \int_{\vartheta(t)} \delta r_i\;(\; f_i \;-\; \rho\ddot{Z}_i\;)\; d\vartheta\; dt \;\; = \tag{3.24}$$
$$\int_{t_1}^{t_2} \int_{\xi(t)} \rho A\;\delta u^T \left\{ \frac{-\mu\;(\;Z \;+\; x\;)}{\|\;\mathbf{Z} \;+\; \mathbf{x}\;\|^3} \;-\; \ddot{Z} \right\} d\xi\; dt \;.$$

As suggested in Ref. 27, a second order Taylor's series expansion will be used to evaluate the gravitational force as $\|\mathbf{x}\| \;/\; \|\mathbf{Z}\| \;\ll 1$.

4.0 Space-Time Discretization of Hamiltonian Equations

An accurate numerical solution procedure is developed from the Hamiltonian variational statement of the equations of motion by incorporating finite element approximation methods for both the space and time dimensions. A space-time finite element approximation of a continuous displacement u can be given as

$$u \simeq \sum_{I=1}^{n_\xi} \sum_{J=1}^{n_t} N_I(\xi)\ N_J(t)\ u_I^{t_J} \qquad (4.1)$$

where n_ξ and n_t are the number of spatial and temporal nodal points, respectively; $N_{I,J}$ are conventional finite element interpolation functions and $u_I^{t_J}$ are the discrete values of u at the spatial node I and time t_J. For interpretation within the present deployment problem, the nodal value is thus the displacement with respect to the node $\bar{X}_I(t_j)$ whose position is prescribed throughout the simulation as a function of the deployment speed. The space-time finite element approximation will be extended to address rotational degrees of freedom R such that finite rotations are properly treated. Given the proper approximations for displacement and rotational variables, the double integration over space and time within the Hamiltonian variational statement can be evaluated such the continuous variational equations are transformed to a set of algebraic equations which are functions of the nodal displacement values $u_I^{t_J}$ and $R_I^{t_J}$. It will be seen that the discrete set of equations are highly nonlinear, and a Newton-Rhapson iteration algorithm must be employed for their solution. To this end, the space-time approximation functions for the displacement and rotational variables are defined in Section 4.1. From the space-time approximations, the form of the discrete equations of motion are presented in Section 4.2, and the solution method for these equations is presented in Section 4.3.

4.1 Space-time Approximation Functions

4.1.1 Space-time approximation of a continuous displacement: As the spatial and temporal derivatives within the Hamiltonian variational statement are no higher than first-order, C_0 continuous approximating functions may be employed in the present analysis. As such, the following linear interpolation in space of a translational displacement u between the spatial nodal values u_1^t and u_2^t at the endpoints of an element of length ℓ at a given instant in time t

$$u^T \simeq u_1^t + \frac{\xi}{\ell}\left(u_2^t - u_1^t\right), \quad 0 \le \xi \le \ell \qquad (4.2)$$

can be combined with a linear interpolation in time between the values $u_i^{t_1}$ and $u_i^{t_2}$ of a spatial node i at the discrete time points t_1 and t_2 where $t_2 = t_1 + h$

$$u_i^t = u_i^{t_1} + \frac{t}{h}\left(u_i^{t_2} - u_i^{t_1}\right), \quad 0 \le t \le h \qquad (4.3)$$

to give the following space-time interpolation of u as

$$\begin{aligned} u \simeq\ & \left(1-\frac{\xi}{\ell}\right)\left(1-\frac{t}{h}\right)u_1^{t_1} + \left(1-\frac{\xi}{\ell}\right)\left(\frac{t}{h}\right)u_1^{t_2} \\ & + \left(\frac{\xi}{\ell}\right)\left(1-\frac{t}{h}\right)u_2^{t_1} + \left(\frac{\xi}{\ell}\right)\left(\frac{t}{h}\right)u_2^{t_2} \end{aligned} \qquad (4.4)$$

4.1.2 Space-time approximation of a continuous rotation: In order to properly treat the rotational degrees of freedom, we define a space-time finite element approximation of a rotation matrix R as follows. The Euler-Chasles theorum states that any finite rotation can be uniquely represent with a rotation angle β and a rotation axis $\mathbf{n}$.[28] From this parameterization, an orthogonal rotation matrix is defined as the matrix exponential of the skew-symmetric tensor defined from the components of the rotation vector $\beta\mathbf{n}$ as (4.5)

$$R = exp\left(\beta\,\tilde{\mathbf{n}}^T\right), \quad \tilde{\mathbf{n}} \equiv \begin{bmatrix} 0 & -n_3 & n_2 \\ n_3 & 0 & -n_1 \\ -n_2 & n_1 & 0 \end{bmatrix}$$

The value of a rotation matrix R between two nodal values R_1^t and R_2^t at an instant in time t will be defined by interpolating the rotation vector $\beta\mathbf{n}$ that represents the relative rotation ΔR between R_1^t and R_2^t. In other words, given the rotation vector $\beta\mathbf{n}$ which represents the relative rotation from nodal orientation R_1 to nodal orientation R_2 as defined by the rotation matrix

$$\Delta R_\ell = R_2^t\, R_1^{t^T}, \qquad (4.6)$$

the interpolation of R between R_1^t and R_2^t is defined by a relative rotation of angle

$$\frac{\xi}{\ell}\beta, \quad 0 \le \xi \le \ell$$

about the same axis of rotation $\mathbf{n}$ as

$$R_\xi = \Delta R_\xi\, R_1^t, \quad \Delta R_\xi = exp\left(\frac{\xi}{\ell}\beta\tilde{\mathbf{n}}^T\right) \qquad (4.7)$$

where ΔR_ξ is the relative rotation matrix corresponding to the rotation vector $\frac{\xi}{\ell}\beta\mathbf{n}$. This interpolation between spatial finite element nodes can be followed by a similar interpolation in time between the temporal values $R_i^{t_1}$ and $R_i^{t_2}$ at a given spatial node i as

$$R_i^t = \Delta R^t\, R_i^{t_1}, \quad \Delta R^t = exp\left(\frac{t}{h}\phi\tilde{\mathbf{m}}^T\right) \qquad (4.8)$$

where ΔR^t is the relative rotation matrix corresponding to the rotation vector

$$\frac{t}{h}\phi\mathbf{m}, \quad 0 \le t \le h$$

and the parameters $\phi\mathbf{m}$ represent the relative rotation from the orientation $R_i^{t_1}$ at time t_1 to the orientation $R_i^{t_2}$ at time t_2 given by the matrix

$$\Delta R^h = R_i^{t_2}\, R_i^{t_1 T}. \qquad (4.9)$$

By compounding the time interpolation with the space interpolation, the space-time interpolation of a finite rotation matrix R is thus defined as

$$R = \Delta R_\xi\, \Delta R^t\, R_1^{t_1}. \qquad (4.10)$$

4.2 Discrete Equations of Motion

From the preceding discussion on the space-time interpolation of the displacement vectors and rotational matrices, a set of discrete equations of motion can be derived by introducing the approximations (4.4) and (4.10) into the Hamiltonian variational statement (3.5). To this end, the discrete form of the interior and boundary inertia operators

(3.6) and (3.10), the internal force operator (3.16), and the external force operator (3.24) are given as follows.

4.2.1 Translational Interior Inertia: The interior inertia term corresponding to the translational displacement of the continuous beam is transformed to the discrete form as

$$\int_{t_1}^{t_2} \int_{\xi} \left\{ \frac{\partial u^T}{\partial t} + V^a \frac{\partial u^T}{\partial \xi} \right\} M \left\{ \frac{\partial \delta u}{\partial t} + V^a \frac{\partial \delta u}{\partial \xi} \right\} d\xi \; dt$$

$$\simeq \left\{ \delta u_d^{t_1 T} \quad \delta u_d^{t_2 T} \right\} \begin{bmatrix} A_{u_{11}} & A_{u_{12}} \\ A_{u_{21}} & A_{u_{22}} \end{bmatrix} \begin{Bmatrix} u_d^{t_1} \\ u_d^{t_2} \end{Bmatrix} \quad (4.11)$$

using the approximation (4.4). In this expression, $u_d^{t_i}$, $i = 1,2$ represents the translational displacements of the entire set of n_ξ spatial finite element nodes at the time limits t_1 and t_2, and

$$\begin{aligned} A_{u_{11}} &= \frac{1}{h} M_1 + M_2 + M_2^T + \frac{h}{4} M_3 \\ A_{u_{12}} &= -\frac{1}{h} M_1 + M_2 - M_2^T + \frac{h}{4} M_3 \\ A_{u_{21}} &= -\frac{1}{h} M_1 - M_2 + M_2^T + \frac{h}{4} M_3 \\ A_{u_{22}} &= \frac{1}{h} M_1 - M_2 - M_2^T + \frac{h}{4} M_3 \end{aligned}$$

are $(3n_\xi) \times (3n_\xi)$ block matrices which are obtained from standard displacement finite element evaluations of the terms

$$\int_{\xi} \rho A \frac{\partial \delta u^T}{\partial t} \frac{\partial u}{\partial t} \, d\xi \simeq \delta u_d \, M_1 \, u_d \quad (4.12)$$

$$\int_{\xi} \rho A \, V^{a^2} \frac{\partial \delta u^T}{\partial \xi} \frac{\partial u}{\partial \xi} \, d\xi \simeq \delta u_d \, M_3 \, u_d \quad (4.13)$$

$$\int_{\xi} \rho A \, V^a \frac{\partial \delta u^T}{\partial t} \frac{\partial u}{\partial \xi} \, d\xi \simeq \delta u_d \, M_2 \, u_d \quad . (4.14)$$

In deriving these approximations, reduced one-point integration methods were employed to evaluate both the integration over the changing spatial domain and the integration over the time interval. It has been shown that in general, an exact evaluation of the space-time finite element approximation for the basic kinematic or *primal* form of Hamilton's law employed within leads to conditionally stable time integration algorithms such that small step sizes may be required to achieve accurate results.[22-24] This type of behavior is similar to the locking phenomenon witnessed during the use of certain elasticity finite elements for static analysis which has been attributed to inconsistencies in the order of approximation of various strain energy terms. As with the locking phenomenon, it was discovered that inaccurate reduced integrations in time of the higher order terms will lead to unconditionally stable time integration algorithms. Space-time finite element discretizations of a *mixed* form of Hamilton's Law have also resulted in algorithms with unconditionally stable numerical behavior.[24,25] The former approach has been adopted in the present analysis, and the latter approach will be investigated in future work.

4.2.2 Rotational Interior Inertia: While the preceding analysis of the discrete approximation for the interior inertia of the translational displacements of the continuous beam is straightforward, the treatment of the interior inertia of the cross-section orientations is much more complicated due to the necessity for a proper treatment of the finite rotations. The term within the interior inertia expression corresponding to the rotational motion of the continuous beam given as

$$\int_{t_1}^{t_2} \int_{\xi} \left\{ \omega^T + V^a \kappa^T \right\} J \left\{ \delta\omega + V^a \kappa \right\} d\xi \; dt$$

is explicitly written in terms of the virtual rotations $\delta\alpha$ as

$$\int_{t_1}^{t_2} \int_{\xi} \left\{ \left\{ \delta\alpha^T + V^a \frac{\partial \delta\alpha^T}{\partial \xi} \right\} J \, \omega_c + \delta\alpha^T \tilde{\omega}_c^T J \, \omega_c \right\} d\xi \; dt \quad (4.15)$$

by incorporating the definitions (3.7) and (3.8) into the above and introducing the definition

$$\omega_c \equiv \omega + V^a \kappa \quad (4.16)$$

to represent the total angular velocity of the local plus convective rates. The space-time finite element approximation of the rotational interior inertia is then represented by

$$\int_{t_1}^{t_2} \int_{\xi} \left\{ \omega^T + V^a \kappa^T \right\} J \left\{ \delta\omega + V^a \kappa \right\} d\xi \; dt$$

$$\simeq \left\{ \delta\alpha_d^{t_1 T} \quad \delta\alpha_d^{t_2 T} \right\} \begin{Bmatrix} A_{\alpha_1} \\ A_{\alpha_2} \end{Bmatrix} \quad (4.17)$$

where $\delta\alpha_d^{t_i}$, $i = 1,2$ represents the virtual rotations of the entire set of spatial finite element nodes at the time limits t_1 and t_2. The $3n_\xi$ components of

$$A_{\alpha_1} = A_{\alpha_1}\left(R_d^{t_1}, R_d^{t_2} \right) , \quad A_{\alpha_2} = A_{\alpha_2}\left(R_d^{t_1}, R_d^{t_2} \right)$$

are nonlinear functions of the set of nodal cross-sectional rotational matrices R_d at the given time limits t_1 and t_2. The form of these vectors is as follows:

$$\begin{aligned} A_{\alpha_1} &= -M_4 + \frac{h}{2} M_5 + \frac{h}{2} M_6 \\ A_{\alpha_2} &= M_4 + \frac{h}{2} M_5 + \frac{h}{2} M_6 \end{aligned}$$

where M_4, M_5, and M_6 are obtained from one-point finite element evaluations of

$$\int_{\xi} \delta\dot{\alpha}^T J \, \omega_c \, d\xi \simeq \delta\dot{\alpha}_d \, M_4 \quad (4.18)$$

$$\int_{\xi} V^a \frac{\partial \, \delta\alpha^T}{\partial \xi} J \, \omega_c \, d\xi \simeq \delta\alpha_d \, M_5 \quad (4.19)$$

$$\int_{\xi} \delta\alpha^T \tilde{\omega}_c^T J \, \omega_c \, d\xi \simeq \delta\alpha_d \, M_6 \quad . \quad (4.20)$$

To obtain the one-point space-time finite element evaluations of (4.18 - 4.20), an evaluation of ω_c at the mid-point in time and at the mid-length of the element must be determined from the nodal rotation matrices R^{t_1} and R^{t_2}. In order to evaluate ω_c in this manner, the local angular velocity ω and element curvature κ are obtained from the

rotational matrix interpolation (4.10) as follows. By differentiating the rotational matrix interpolation (4.10), the curvature of a beam finite element can be derived as the following constant

$$\tilde{\kappa}^T \equiv \frac{\partial R}{\partial \xi} R^T = \frac{\beta}{\ell} \tilde{\mathbf{n}}^T \quad (4.21)$$

where $\beta\mathbf{n}$ is the rotation vector parameterization of the relative rotation ΔR_ℓ between two spatial finite element nodes as defined in (4.6). This element curvature will be evaluated once at the mid point of the time limits t_1 and t_2 of step size h such that the parameters β and $\mathbf{n}$ will be defined from nodal rotation matrices $R_i^{t_h}$ where $t_h = t_1 + h/2$. To accomplish this, the nodal matrices $R_i^{t_h}$ are obtained by interpolating between $R_i^{t_1}$ and $R_i^{t_2}$ via

$$R_i^{t_h} = \Delta R_i^{\frac{h}{2}} R_i^{t_1} , \quad \Delta R_i^{\frac{h}{2}} = exp\left(\frac{\phi_i}{2} \tilde{\mathbf{m}}_i^T \right) \quad (4.22)$$

where rotational parameters $\phi_i\mathbf{m}_i$ represent the relative rotation between time t_1 and t_2 of the nodal orientations as defined by ΔR^h in (4.9). Given the mid-time interpolation $R_i^{t_h}$ for the cross-section orientations at the spatial finite element nodes, the parameters β and $\mathbf{n}$ used to define the element curvature are then defined from the relative orientation of node 2 with respect to node 1 of a spatial finite element at the time t^h as

$$\Delta R_\ell^{t_h} = R_2^{t_h} \left(R_1^{t_h} \right)^T = exp\left(\beta \tilde{\mathbf{n}}^T \right) . \quad (4.23)$$

It is important to note that as $\mathbf{n}$ is extracted from the matrix ΔR defined by (4.23), the components of $\mathbf{n}$ are defined with respect to the $R_1^{t_h}$ reference frame. Therefore, the curvature definition given in (4.21) has components defined with respect to the reference frame $R_1^{t_h}$. In order to be consistent with the reduced integration concept used through the integral evaluations, the curvature must be evaluated or defined at a reference frame mid-way between the two spatial nodal references. This mid-element reference frame can be defined as

$$R_{\ell/2}^{t_h} = \Delta R_{\ell/2} R_1^{t_h} , \quad \Delta R_{\ell/2} = exp\left(\frac{\beta}{2} \tilde{\mathbf{n}}^T \right) \quad (4.24)$$

and the curvature as referred to this mid-element frame is given as

$$\kappa = \frac{\beta}{\ell} \Delta R_{\ell/2} \mathbf{n} \quad (4.25)$$

Using similar concepts, the angular velocity of the beam mid-element reference frame at the mid-time point t_h is defined as follows. We begin by differentiating the rotational matrix approximation (4.10) in time to define the angular velocity ω_i at a spatial node i as

$$\tilde{\omega}_i^T \equiv \frac{dR_i}{dt} R_i^T = \frac{\phi_i}{h} \tilde{\mathbf{m}}_i^T . \quad (4.26)$$

The parameters $\phi_i\mathbf{m}_i$ represent the relative rotation between time t_1 and t_2 of the nodal orientations as defined by (4.9). From this definition, the components of $\mathbf{m}_i$ are based on the reference frame $R_i^{t_1}$. To be consistent with the evaluation of the element curvature, this nodal angular velocity is first transformed to the reference frame $R_i^{t_h}$ via

$$\omega_i = \frac{\phi_i}{h} \Delta R_i^{\frac{h}{2}} \mathbf{m}_i . \quad (4.27)$$

The body-fixed nodal angular velocities are then transformed again to a mid-element reference $R_{\frac{\ell}{2}}^{t_h}$ as opposed to a nodal references via

$$\omega_{m_1} = \Delta R_{\frac{\ell}{2}} \omega_1 , \quad \omega_{m_2} = \Delta R_{\frac{\ell}{2}}^T \omega_2 \quad (4.28)$$

and we finally take the average of these two quantities

$$\omega = \frac{1}{2} (\omega_{m_1} + \omega_{m_2}) \quad (4.29)$$

to define the mid-element, mid-time angular velocity.

It remains to describe how to obtain the rotation vectors $\beta\mathbf{n}$ and $\phi\mathbf{m}$ from a given ΔR matrix. In the present work, Euler parameters are used to represent the given rotation matrices $R_i^{t_j}$ throughout the transient integration procedure. The Euler parameters $\{\Delta q_0, \Delta\mathbf{q}\}$ representing a relative rotation matrix ΔR between two general orientations R_I and R_J can be computed directly from the nodal Euler parameters $\{q_{0_I}, \mathbf{q}_I\}$ and $\{q_{0_J}, \mathbf{q}_J\}$ representing R_I and R_J, respectively, via

$$\Delta q_0 = q_{0_I} q_{0_J} + \mathbf{q}_I \cdot \mathbf{q}_J \quad (4.30)$$

$$\Delta\mathbf{q} = -q_{0_J} \mathbf{q}_I + q_{0_I} \mathbf{q}_J - \mathbf{q}_I \times \mathbf{q}_J . \quad (4.31)$$

Given the Euler parameters of the relative rotation matrix ΔR, the rotational vector can be accurately determined from

$$\beta = 2\, sin^{-1} (\| \Delta\mathbf{q} \|) , \quad \mathbf{n} = \frac{\Delta\mathbf{q}}{\| \Delta\mathbf{q} \|} . \quad (4.32)$$

In addition, the Euler parameters $\{\Delta q_{0_{\frac{\ell}{2}}}, \Delta\mathbf{q}_{\frac{\ell}{2}}\}$ corresponding to a relative rotation of $\frac{\beta}{2}\mathbf{n}$ are directly determined from Euler parameters $\{\Delta q_0, \Delta\mathbf{q}\}$ as (4.33)

$$\Delta q_{0_{\frac{\ell}{2}}} = \sqrt{\frac{1 + \Delta q_0}{2}} , \quad \Delta\mathbf{q}_{\frac{\ell}{2}} = \frac{\Delta\mathbf{q}}{2\, \Delta q_{0_{\frac{\ell}{2}}}} ,$$

and $\Delta R_{\frac{\ell}{2}}$ is directly formed given these Euler parameters. This completes the description of the reduced integration, mid-time mid-element evaluation of the angular velocity ω and curvature κ necessary to evaluate the nonlinear interior term of the inertia operator corresponding to the rotational degrees of freedom.

4.2.3 Boundary Inertia Terms: To complete the numerical evaluation of the Hamiltonian inertia terms, it remains to discuss the temporal boundary term given by (3.10). This boundary term can be rewritten as

$$\int_{\xi(t)} \{ \delta u^T \; \delta\alpha^T \} \begin{Bmatrix} P_{\dot{u}} \\ P_\omega \end{Bmatrix} d\xi \Big|_{t_1}^{t_2} \quad (4.34)$$

where

$$\begin{Bmatrix} P_{\dot{u}} \\ P_{\omega} \end{Bmatrix} \equiv \begin{Bmatrix} M \{ \dot{u} + V^a \frac{\partial u}{\partial \xi} \} \\ J \{ \omega + V^a \kappa \} \end{Bmatrix} \tag{4.35}$$

is the vector of generalized momenta. To achieve a correct numerical evaluation of the boundary term, the generalized momenta must be evaluated exactly as it stands and must not be approximated in any manner in the time domain. As such, the discrete boundary term is given as

$$\{ \delta u_d^{t_1 T} \ \delta u_d^{t_2 T} \} \begin{bmatrix} -C^{t_1} & 0 \\ 0 & C^{t_2} \end{bmatrix} \begin{Bmatrix} P_{\dot{u}_d}^{t_1} \\ P_{\dot{u}_d}^{t_2} \end{Bmatrix} +$$

$$\{ \delta \alpha_d^{t_1 T} \ \delta \alpha_d^{t_2 T} \} \begin{bmatrix} -C^{t_1} & 0 \\ 0 & C^{t_2} \end{bmatrix} \begin{Bmatrix} P_{\omega_d}^{t_1} \\ P_{\omega_d}^{t_2} \end{Bmatrix} \tag{4.36}$$

where the matrix C^{t_i} is obtained from an exact finite element evaluation of the spatial integral over the length ξ^{t_i} given in (4.34) in which the virtual displacements δu and $\delta \alpha$ are considered to be independent of the corresponding generalized momenta $P_{\dot{u}}$ and P_{ω}. Such an exact evaluation is to recover of the momenta at the end of each time step based on physical principles by providing an exact discrete interpretation of the impulse-momentum principle.

4.2.4 Internal Force: The space-time finite element approximation of the internal force will be represented as

$$\int_{t_1}^{t_2} \int_{\xi(t)} \{ \delta u^T \ \delta \alpha^T \} \ [\ B \ ]^T \begin{Bmatrix} N_{\gamma} \\ M_{\kappa} \end{Bmatrix} d\xi \ dt \simeq \tag{4.37}$$

$$\{ \delta u_d^{t_1 T} \ \delta u_d^{t_2 T} \} \begin{Bmatrix} \frac{h}{2} S_u \\ \frac{h}{2} S_u \end{Bmatrix} + \{ \delta \alpha_d^{t_1 T} \ \delta \alpha_d^{t_2 T} \} \begin{Bmatrix} \frac{h}{2} S_{\alpha} \\ \frac{h}{2} S_{\alpha} \end{Bmatrix}$$

The terms S_u and S_{α} represent a nonlinear finite element evaluation of the internal force of the beam as (4.38)

$$\int_{\xi(t)} \{ \delta u^T \ \delta \alpha^T \} \ [\ B \ ]^T \begin{Bmatrix} N_{\gamma} \\ M_{\kappa} \end{Bmatrix} d\xi \simeq \delta u_d \ S_u + \delta \alpha_d \ S_{\alpha}$$

from a given set of nodal displacements and nodal rotations

$$S_u = S_u (u_d, R_d) \ , \qquad S_{\alpha} = S_{\alpha} (u_d, R_d) \ .$$

Specific details regarding this spatial finite element evaluation of the beam internal force is discussed in previous work by the present authors.[18–20] In arriving at (4.37), a one-point gaussian integration has been used to evaluate the integral over the time domain in order to achieve an unconditionally stable time integration algorithm. This results in the factor $h/2$, and the evaluation of S_u and S_{α} using discrete nodal displacements and rotations at the mid-point in time t^h. The mid-time nodal displacements are defined as the average of u^{t_1} and u^{t_2}, and the mid-time nodal rotations are defined as described in (4.23).

4.2.5 External Force: In a similar manner, the space-time approximation of the external force due to orbit in a gravitational field is given as

$$\int_{t_1}^{t_2} \int_{\xi(t)} \rho A \ \delta u^T \left\{ -\frac{\mu (Z + x)}{\| \mathbf{Z} + \mathbf{x} \|^3} - \ddot{Z} \right\} d\xi \ dt$$

$$\simeq \{ \delta u_d^{t_1 T} \ \delta u_d^{t_2 T} \} \begin{Bmatrix} \frac{h}{2} F_G \\ \frac{h}{2} F_G \end{Bmatrix} \tag{4.39}$$

where F_G corresponds to a standard displacement finite element evaluation of the gravitational force (4.40)

$$\int_{\xi(t)} \left\{ \rho A \ \delta u^T \frac{-\mu \{ Z + x \}^T}{\| \mathbf{Z} + \mathbf{x} \|^3} - \ddot{Z}^T \right\} d\xi \simeq \delta u_d^T F_G \ .$$

As with the internal force evaluation, a one-point gaussian integration in time is employed to arrive at (4.39), and thus F_G from the displacement average $x_d^{t_h} = (x_d^{t_1} + x_d^{t_2}) / 2$.

4.3 Solution of Discrete Equations of Motion

The space-time finite element approximation of the Hamiltonian equations of motion results in the following step-by-step implicit time integration algorithm. By combining all of the developments of the previous section, we arrive at the following set of nonlinear algebraic equations

(4.41)

$$A_{u_{11}} u^{t_1} + A_{u_{12}} u^{t_2} - \frac{h}{2} S_u + \frac{h}{2} F_G = -C^{t_1} P_{\dot{u}}^{t_1}$$

$$A_{\alpha_1} - \frac{h}{2} S_{\alpha} = -C^{t_1} P_{\omega}^{t_1} \tag{4.42}$$

(4.43)

$$A_{u_{21}} u^{t_1} + A_{u_{22}} u^{t_2} - \frac{h}{2} S_u + \frac{h}{2} F_G = C^{t_2} P_{\dot{u}}^{t_2}$$

$$A_{\alpha_2} - \frac{h}{2} S_{\alpha} = C^{t_2} P_{\omega}^{t_2} \tag{4.44}$$

as the discrete approximation of the Hamilton variational statement where the subscript d on the nodal variables has been dropped. The terms A_{α_1} and A_{α_2} are nonlinear functions of the nodal rotations $\{R^{t_1}, R^{t_2}\}$; the terms S_u and S_{α} are nonlinear functions of the nodal displacements and rotations $\{u^{t_1}, R^{t_1}, u^{t_2}, R^{t_2}\}$ and couple the translational motion with the rotational motion; the term F_G is a nonlinear function of the nodal displacements $\{u^{t_1}, u^{t_2}\}$, and the remaining terms in the above equations are linear as shown.

It is readily seen that, given a set of initial conditions for the discrete generalized displacements $\{u^{t_1}, R^{t_1}\}$ and the generalized momenta $\{P_{\dot{u}}, P_{\omega}\}$, the first two equations (4.41) and (4.42) can be solved for the generalized displacements at the time t_2. Given this solution for u^{t_2} and R^{t_2}, the second two equations (4.43) and (4.44) can then be solved for the generalized momenta $P_{\dot{u}}$ and P_{ω} at time t_2. These new solutions can then be used as initial conditions for the next step in time, and the process can be repeated to give a one-step implicit time integration algorithm.

As the first two equations are nonlinear algebraic equations, a Newton-Rhapson iterative procedure must be employed to obtain the solution for the generalized displacements u^{t_2} and R^{t_2}. To this end, a linearized set of equations

$$E_{(k+1)} \left\{ \begin{array}{c} \Delta u^{t_2} \\ \Delta \alpha^{t_2} \end{array} \right\}_{(k+1)} = - \left\{ \begin{array}{c} r_u \\ r_\alpha \end{array} \right\}_{(k+1)} \tag{4.45}$$

where

$$\begin{aligned} r_{u_{(k+1)}} &= A_{u_{11}}\, u^{t_1} + A_{u_{12}}\, u^{t_2}_{(k+1)} - \frac{h}{2}\, S_{u_{(k+1)}} \\ &\quad + \frac{h}{2} F_{G_{(k+1)}} + C^{t_1}\, P_u^{t_1} \\ r_{\alpha_{(k+1)}} &= A_{\alpha_{1\ (k+1)}} - \frac{h}{2}\, S_{\alpha\ (k+1)} + C^{t_1}\, P_\omega^{t_1} \end{aligned}$$

are the residual errors of the algebraic equations (4.41) and (4.42) at a given solution $u^{t_2}_{(k+1)}$ and $R^{t_2}_{(k+1)}$, and

$$E \equiv \left[\begin{array}{cc} D\, r_u \cdot \Delta u & D\, r_u \cdot \Delta \alpha \\ D\, r_\alpha \cdot \Delta u & D\, r_\alpha \cdot \Delta \alpha \end{array} \right] \tag{4.46}$$

is the tangent solution matrix. To obtain this solution matrix, we need consistent linearizations and subsequent finite element evaluations of the nonlinear rotational inertia terms

$$\begin{aligned} \delta F^I_{\alpha_1} &\equiv \int_\xi \delta\dot\alpha^T\ J\ (\ \omega + V^a \kappa\ )\ d\xi \qquad (4.47) \\ \delta F^I_{\alpha_2} &\equiv \int_\xi V^a\, \frac{\partial\, \delta\alpha^T}{\partial \xi}\, J\ (\ \omega + V^a \kappa\ )\ d\xi \\ \delta F^I_{\alpha_3} &\equiv \int_\xi \delta\alpha^T (\ \tilde\omega^T + V^a \tilde\kappa^T\ )\ J\ (\ \omega + V^a \kappa\ )\ d\xi\ , \end{aligned}$$

the virtual work of the nonlinear internal force

$$\delta F^S \equiv \int_{\xi(t)} \{\ \delta u^T\ \delta\alpha^T\ \}\ [\ B\ ]^T \left\{ \begin{array}{c} N_\gamma \\ M_\kappa \end{array} \right\} d\xi \quad ,$$

and the virtual work of the gravitational external force.

$$\delta F^G = \int_{\xi(t)} \rho A\, \delta u^T \left\{ \frac{-\mu\ \{\ Z + x\ \}^T}{\|\ \mathbf{Z} + \mathbf{x}\ \|^3} - \ddot Z \right\} d\xi \quad .$$

To linearize the rotational inertia, a linear perturbation of the angular velocity and curvature vector and tensor have been derived such that consistency with the theory of finite rotations is maintained.[12-14,16] These linearizations are given as

$$\begin{aligned} D\tilde\omega \cdot \Delta\alpha &= \Delta\dot{\tilde\alpha} + \tilde\omega\, \Delta\tilde\alpha - \Delta\tilde\alpha\, \tilde\omega \qquad (4.48) \\ D\tilde\kappa \cdot \Delta\alpha &= \Delta\dot{\tilde\alpha} + \tilde\kappa\, \Delta\tilde\alpha - \Delta\tilde\alpha\, \tilde\kappa \qquad (4.49) \\ D\omega \cdot \Delta\alpha &= \Delta\dot\alpha + \tilde\omega \Delta\alpha \qquad (4.50) \\ D\kappa \cdot \Delta\alpha &= \Delta\dot\alpha + \tilde\kappa \Delta\alpha \qquad (4.51) \end{aligned}$$

for the corresponding vectors where $\Delta\alpha$ are linear, infinitesimal angles of rotation about a set of basis vectors R^n corresponding to a state of equilibrium. When these linearizations are used within the expressions (4.47), the following tangent operators

$$\begin{aligned} \delta K^I_{\alpha_1} &= \int_\xi \delta\dot\alpha^T \left\{ J \frac{\partial \Delta\alpha}{\partial t} + V^a J \frac{\partial \Delta\alpha}{\partial \xi} + C_1 \Delta\alpha \right\} d\xi \\ \delta K^I_{\alpha_2} &= \int_\xi \frac{\partial \delta\alpha^T}{\partial \xi} \left\{ V^a J \frac{\partial \Delta\alpha}{\partial t} + V^{a^2} J \frac{\partial \Delta\alpha}{\partial \xi} + V^a C_1 \Delta\alpha \right\} d\xi \\ \delta K^I_{\alpha_3} &= \int_\xi \delta\alpha^T \left\{ C_2 \frac{\partial \Delta\alpha}{\partial t} + V^a C_2 \frac{\partial \Delta\alpha}{\partial \xi} + C_3 \Delta\alpha \right\} d\xi \end{aligned}$$

are obtained for $\delta F^I_{\alpha_1}$,$\delta F^I_{\alpha_2}$,and $\delta F^I_{\alpha_3}$, respectively, where

$$\begin{aligned} C_1 &= J\, \tilde\omega + V^a\, J\, \tilde\kappa \\ C_2 &= \tilde\omega^T J + \widetilde{J\omega} + V^a\, (\ \tilde\kappa^T J + \widetilde{J\kappa}\ ) \\ C_3 &= \tilde\omega^T J\, \tilde\omega + \widetilde{J\omega} + \\ &\quad V^a\, (\ \tilde\omega^T J\, \tilde\kappa + \widetilde{J\kappa}\, \tilde\omega + \tilde\kappa^T J\, \tilde\omega + \widetilde{J\omega}\, \tilde\kappa\ ) \\ &\quad + V^{a^2}\, (\ \tilde\kappa^T J\, \tilde\kappa + \widetilde{J\kappa}\, \tilde\kappa\ ) \quad . \end{aligned}$$

Spatial finite element techniques which are consistent with the reduced integration techniques used to evaluate the residuals are then used to obtain discrete tangent matrices from the above continuous operators as

$$\delta K^I_{\alpha_1} + \delta K^I_{\alpha_1} + \delta K^I_{\alpha_1} \simeq \delta\alpha_d^T\ [\ K^I\ ]\ \Delta\alpha_d \quad .$$

The tangent stiffness operator and tangent stiffness matrix for δF^S is derived in Ref. 18, and will be represented here as

$$\delta K^S \simeq \{\ \delta u_d^T \quad \delta\alpha_d^T\ \}\ [\ K^S\ ] \left\{ \begin{array}{c} \Delta u \\ \Delta\alpha \end{array} \right\} \quad .$$

Finally, the tangent stiffness operator and matrix for the gravitational force δF^G is given as

$$\begin{aligned} \delta K^G &= \delta u^T \left\{ -\frac{1}{\|Z\|^3}\, I + \frac{3Z \cdot x}{\|Z\|^5} + \frac{3xZ^T}{\|Z\|^5} \right. \\ &\quad \left. + \frac{3Z(Z+x)^T}{\|Z\|^5} + \frac{15(Z \cdot x) Z Z^T}{\|Z\|^7} \right\} \Delta u \\ &\simeq \delta u_d\ [\ K^G\ ]\ \Delta u_d \quad . \end{aligned}$$

From this overview, the solution matrix for the Newton-Rhapson iteration procedure is given as

$$E = \left[\begin{array}{cc} A_{u_12} - \frac{h}{4} K^S_{uu} + \frac{h}{4} K^G & -\frac{h}{4} K^S_{u\alpha} \\ -\frac{h}{4} K^{S\,T}_{u\alpha} & K^I - \frac{h}{4} K^S_{\alpha\alpha} \end{array} \right] .$$

The linearized equations are solved at each iteration for incremental displacements Δu^{t_2} and incremental rotations

$\Delta\alpha^{t_2}$, and these incremental solutions then update the displacements u^{t_2} and rotations R^{t_2} via

$$u_{(k+1)}^{\ t_2} = u_{(k)}^{\ t_2} + \Delta u^{t_2}$$
$$R_{(k+1)}^{\ t_2} = exp\,(\,\Delta\tilde{\alpha}^{t_2}{}^{T}\,)\,R_{(k)}^{\ t_2}$$

After a converged solution for u^{t_2} and R^{t_2} is obtained, the generalized momenta $P_u^{t_2}$ and $P_\omega^{t_2}$ is obtained from a direct solution of (4.43) and (4.44).

5.0 Results

We now give some numerical results of the proposed formulation and computational solution procedure. To illustrate the capabilities of the present computational methodology, the case of a two-boom gravity gradient stabilized satellite traversing a circular orbit is considered. A simple yet realistic model of the satellite configuration is given as follows. The central body of the satellite is modeled with two, standard non-deploying beam finite elements of length 10 m with the parameters $\rho A = 2.289$ kg/m, $EA = 2.47 \times 10^7$ N, $EI_2 = EI_3 = 4.8 \times 10^6$ Nm^2, $\rho I_2 = \rho I_3 = .45$ kgm. The two appendages are cantilevered to each end of the beam representing the central body and are modeled with moving node finite elements such that each appendage extends outward from the central body to a total length of 150 m. The appendages are much more flexible than the central body, and the appendage parameters given as $\rho A = .023024$ kg/m, $EA = 2.14 \times 10^3$ N, $EI_2 = EI_3 = 7.85$ Nm^2, $\rho I_2 = \rho I_3 = 8.45 \times 10^{-5}$ kgm coincide with the physical characteristics of the RAE antennae.[7] The mid-node of the two-finite element central body which coincides with the center of mass of the satellite traverses the orbit trajectory. The center of mass is initially located at a distance of $\mathbf{Z}_0 = 6000\ km\ \mathbf{e}_1$ from the center of the Earth, and an initial velocity of $\dot{\mathbf{Z}}_0\sqrt{(\,\mu/Z_0\,)}\,\mathbf{e}_2$ is given such that the center of mass will traverse a circular orbit in the $\mathbf{e}_1 - \mathbf{e}_2$ plane of the inertial reference frame. The gravitational constant μ is given as $\mu = 3.984 \times 10^{14}$ Nm^2/kg. The three-axis librational and vibrational response of the satellite during and after deployment of the flexible appendages is given for different deployment speeds and different disturbances in the initial orientation of the satellite when the deployment is initiated. The main objective was to get some sense of the interaction between the satellite librations and the appendage deformations due to various deployment speeds.

The libration response of the central body is defined by the successive Eulerian rotations of pitch Φ, roll Θ, and yaw Λ to orient the body-fixed axis $\mathbf{b}_3$, $\mathbf{b}_2$, and $\mathbf{b}_1$ attached to the cross-section at the mid-node of the central body with respect to the orbiting reference $\{\mathbf{o}_1, \mathbf{o}_2, \mathbf{o}_3\}$ as shown in Figure 5, where the plane of the orbit coincides with the $\mathbf{e}_1 - \mathbf{e}_2$ plane of the inertial reference frame, $\mathbf{o}_1$ is aligned with the local vertical $\mathbf{Z}$, $\mathbf{o}_3$ is normal to the orbit plane, and $\mathbf{o}_2 = \mathbf{o}_3 \times \mathbf{o}_1$. In Figures 6 and 7, we compare the pitch response of a satellite in which an initial disturbance of rotation $\Theta_0 = 15^o$ about $\mathbf{o}_2$ such that the satellite is oriented 15^o out of the plane of the orbit when the deployment of the appendages is initiated. For the various deployment speeds $V = .1, .15, .3, .5$,and 2.0 m/s, it takes 1500,1000,750,300, and 75 sec for the appendages to fully extend. The time the satellite with the deploying appendages is compard to the response of a satellite in which the appendages are fully extended from the start. It is seen that as the deployment speed increases, the effect of deployment on the libration response is decreased. It is also seen that the initial satellite orientation 15° out of the orbit plane causes much larger angle librations in the orbit plane. In Figure 8, the pitch libration response is compared for an initial satellite orientation of 15° from the local vertical in the orbit plane with the 15° out of plane initial orientation, and it is seen that the large pitch librations result from either disturbance. Figure 9 compares the pitch response of a rigid satellite beam model with the flexible models for the initial 15° out of plane initial orientation for the fully extended case and one deploying case of speed V = .1 m/s. It is seen that the response of the fully extended case barely deviates from the rigid model response, whereas a noticeable change occurred for the deploying case. Figures 10 and 11 repeat the analysis of Figures 6 and 7 for the roll libration response.

The appendage deformations are defined as the displacement of the tip of the appendage as seen with respect to the body-fixed bases $\{\mathbf{b}_1, \mathbf{b}_2, \mathbf{b}_3\}$ at the center of the satellite hub. In Figures 12 and 13, the $\mathbf{b}_2$ and $\mathbf{b}_3$ components of the tip displacements for the above analyses are shown. It is seen that much greater appendage displacements occur as a result of deployment as Figure 14 shows the displacement response for the same initial orientation of a satellite in which the appendages are fully extended from the outset. Figure 15 and Figure 16 then show that the magnitude of the tip displacements can be reduced if the deployment velocity is cut in half just 10 m before the 150 m appendage is fully extended. Finally, Figure 17 shows the high frequency appendage vibrations which result as the deployment speed is increased even further.

Concluding Remarks

A general finite element model which treats the transient and steady state effects of the deployment of a flexible appendage from a rotating and orbiting base has been developed. The key to the formulation is the introduction of a variable finite element reference grid which incorporates the dynamics of deployment within a geometrically nonlinear spatial beam model. The computational methodology is then derived from a space-time finite element discretization of a Hamiltonian

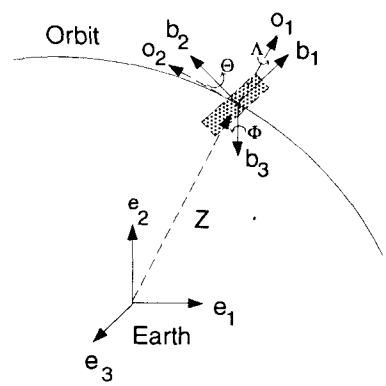

Figure 5: Reference Orientations

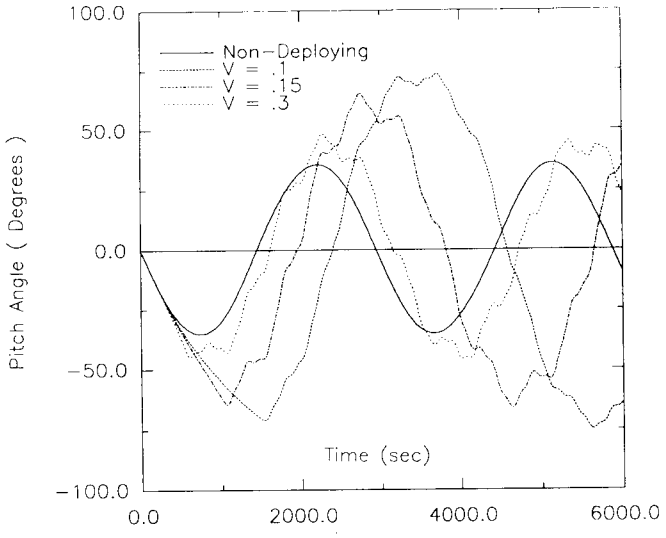

Figure 6: Pitch librations of various deployment speeds.

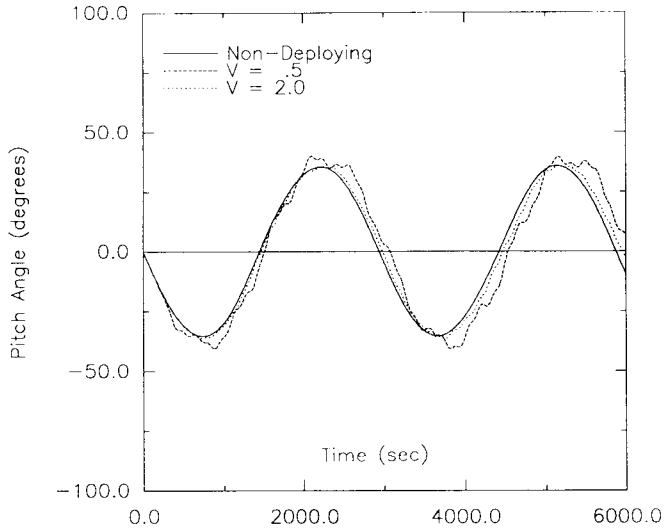

Figure 7: Pitch librations of various deployment speeds.

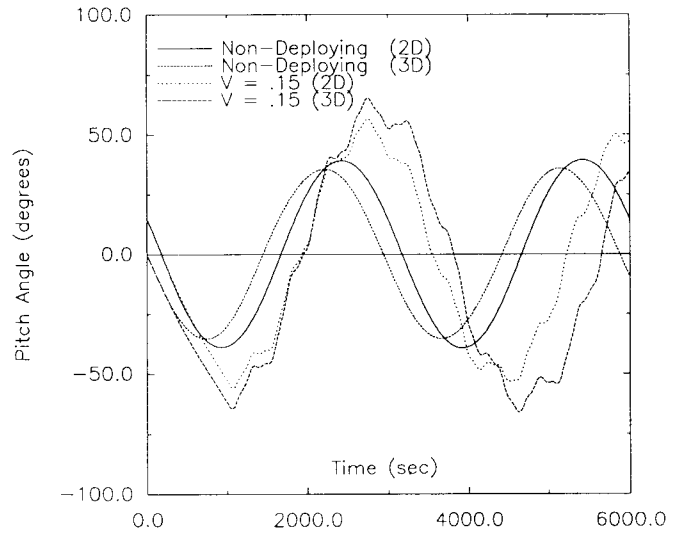

Figure 8: Pitch librations for $\Phi_0 = 15^o$ (2D) vs. $\Theta_0 = 15^o$ (3D).

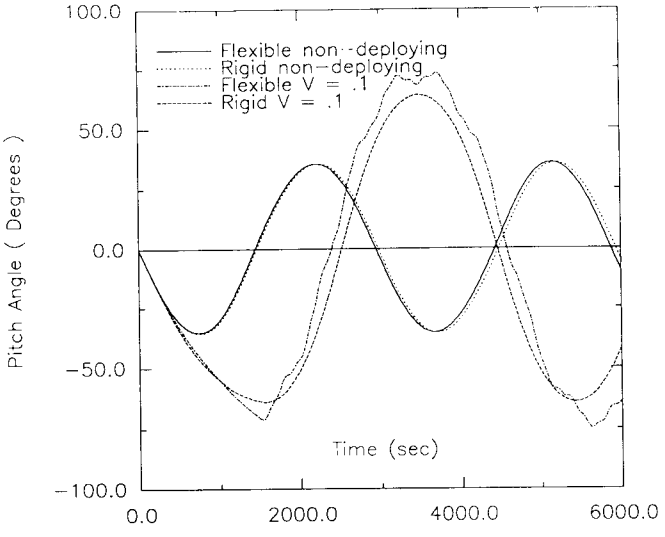

Figure 9: Pitch librations rigid vs. flexible model.

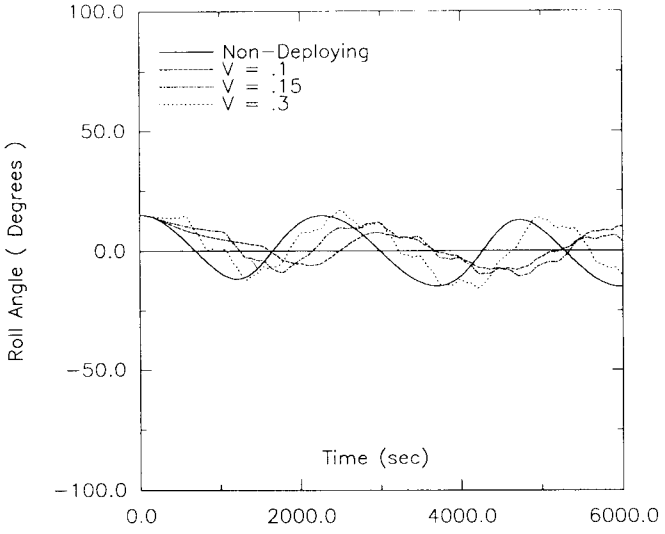

Figure 10: Roll librations of various deployment speeds.

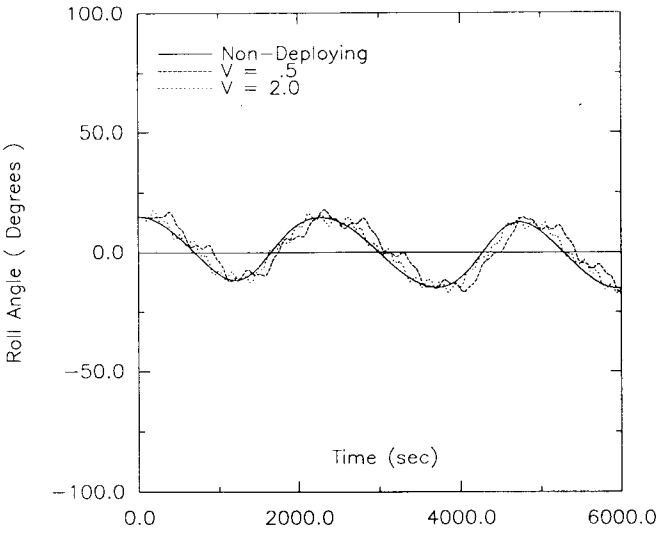

Figure 11: Roll librations of various deployment speeds.

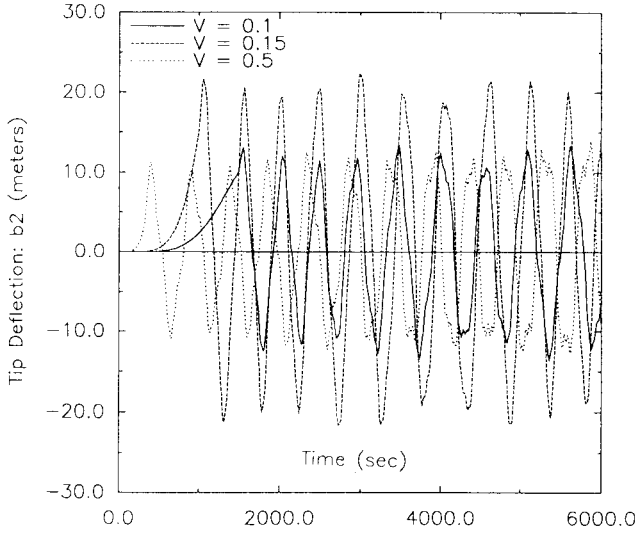

Figure 12: Tip deflections of various deployment speeds ($\mathbf{b_2}$).

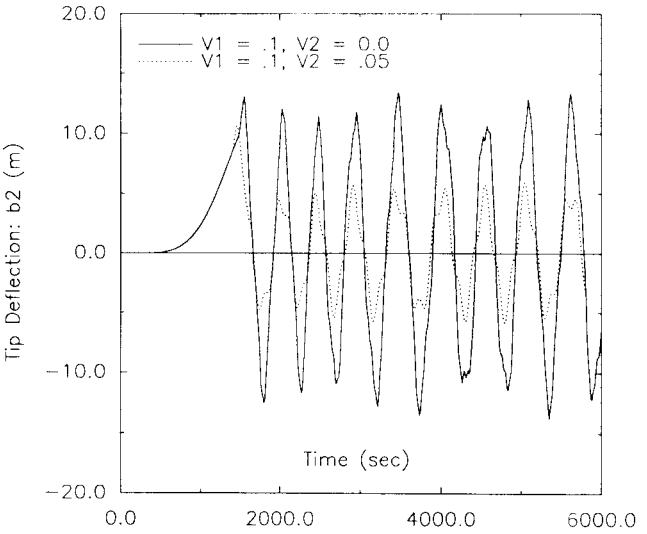

Figure 15: Tip deflections with speed reduced ($\mathbf{b_2}$).

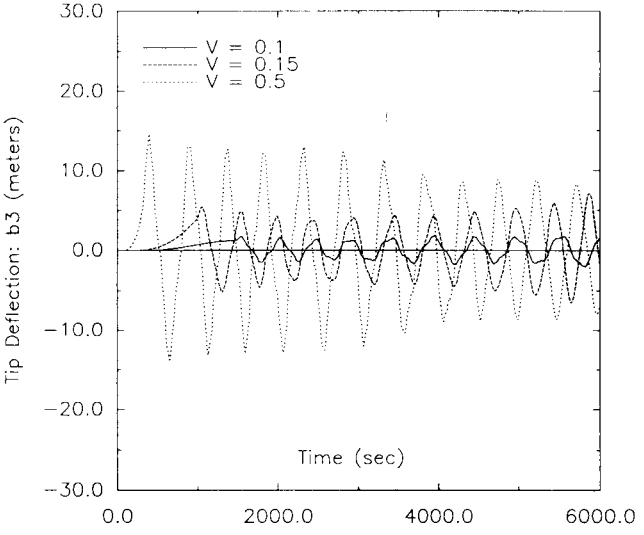

Figure 13: Tip deflections of various deployment speeds ($\mathbf{b_3}$).

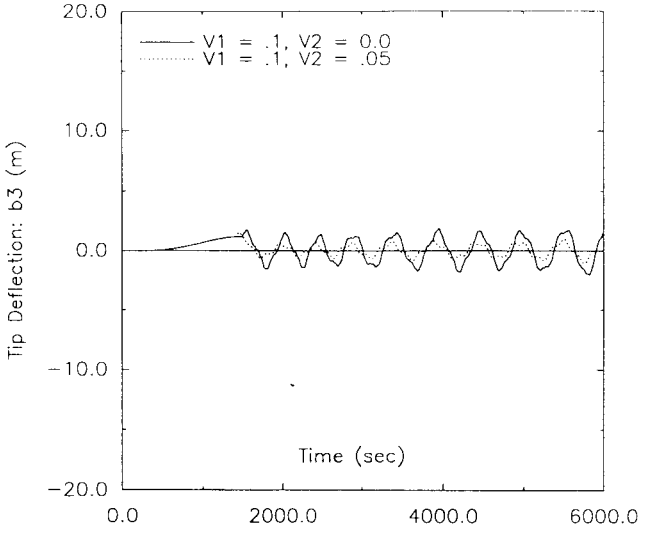

Figure 16: Tip deflections with speed reduced ($\mathbf{b_3}$).

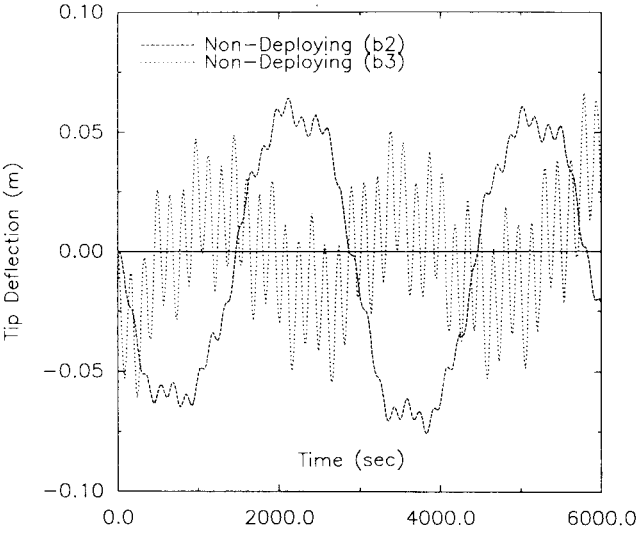

Figure 14: Tip deflections of fully extended satellite.

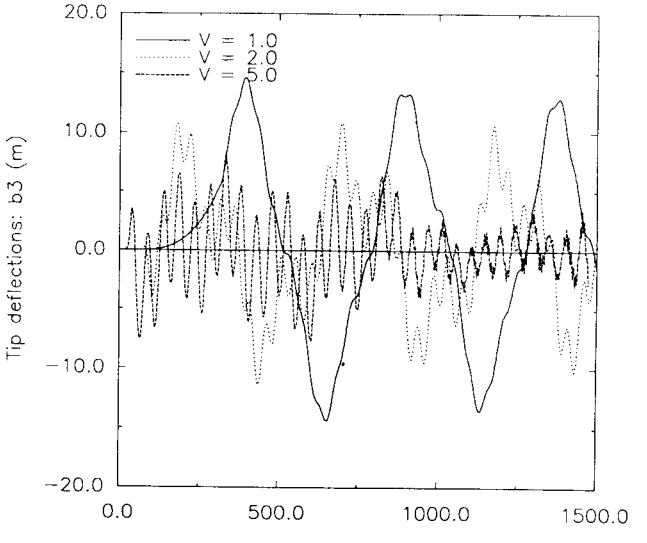

Figure 17: High speed tip deflections.

variational formulation. Computational results of the formulation show significant differences between the libration and vibration response of gravity gradient satellites which deploy flexible appendages as compared to the response of satellites with appendages fully extended from the onset, and the deployment of appendages continues to affect the system response long after the extension is halted.

Acknowledgements

The work reported herein was supported by the NASA/Langley Research Center underGrant NAG-1-756, the Space Project Office of the Shimuzu Corporation, and Jet Propulsion Laboratory.

References

[1]Cloutier, G. J., "Dynamics of Deployment of Extendible Booms from Spinning Space Vehicles," *J. Spacecraft and Rockets*, Vol. 5, 1968, pp. 547-552.

[2]Sellappan, R., and Bainum, P. M., "Dynamics of Spin-Stabilized Spacecraft During Deployment of Telescoping Appendages," *J. Spacecraft and Rockets*, Vol. 13, 1976, pp. 605-610.

[3]Bowers, E. J., and Williams, C. E., "Optimization of RAE Satellite Boom Deployment Timing," *J. Spacecraft and Rockets*, Vol. 7, 1970, pp. 1057-1062.

[4] Cherchas, D. B., "Dynamics of Spin-Stabilized Satellites during Extension of Long Flexible Booms," *J. Spacecraft and Rockets*, Vol. 8, 1971, pp. 802-804.

[5]Ibrahim, A. E. and Misra, A. K., "Attitude Dynamics of a Satellite During Deployment of Large Plate-Type Structures," *J. Guidance, Control, and Dynamics*, Vol. 5, 1982, pp. 442-447.

[6]Lips, K. W., and Modi, V. J., "Transient Attitude Dynamics of Satellites with Deploying Flexible Appendages," *Acta Astronautica*, Vol. 5, 1978, pp. 797-815.

[7]Lips, K. W., and Modi, V. J., "Three-Dimensional Response Characteristics for Spacecraft with Deploying Flexible Appendages," *J. Guidance and Control*, Vol. 4, 1981, pp. 650-656.

[8]Modi, V. J., and Ibrahim, A. M., "A General Formulation for Librational Dynamics of Spacecraft with Deploying Appendages," *J. Guidance, Control, and Dynamics*, Vol. 7, 1984, pp. 563-569.

[9]Banerjee, A. K., and Kane, T. R., "Extrusion of a Beam from a Rotating Base," *J. Guidance, Control, and Dynamics*, Vol. 12, 1989, pp. 140-146.

[10]Mansfield, L. and Simmonds, J. G., "The Reverse Spaghetti Problem: Drooping Motion of an Elastica Issuing from a Horizontal Guide," *J. Appl. Mech.*, Vol. 54, 1987, pp. 147-150.

[11]Downer, J. D., and Park, K. C., "Formulation and Solution of Inverse Spaghetti Problem: Application to Beam Deployment Dynamics," Proceedings the 1991 AIAA Structures, Dynamics, and Materials Conference, Baltimore, Maryland, April 8-10, 1991.

[12]Simo, J. C., "A Finite Strain Beam Formulation. The Three-Dimensional Dynamic Problem. Part I," *Computer Methods in Applied Mechanics and Engineering*, Vol. 49, 1985, pp. 55-70.

[13]Simo, J. C. and Vu Quoc, L., "Three Dimensional Finite Strain Rod Model. Part II: Computational Aspects," *Computer Methods in Applied Mechanics and Engineering*, Vol. 58, 1986, pp. 79-116.

[14]Simo, J. C. and Vu Quoc, L., "On the Dynamics in Space of Rods Undergoing Large Motions - A Geometrically Exact Approach," *Computer Methods in Applied Mechanics and Engineering*, Vol. 66, 1988, pp. 125-161.

[15]Hodges, D. H., "A Mixed Variational Formulation Based on Exact Intrinsic Equations for Dynamics of Moving Beams," *Internation Journal of Solids and Structures*, Vol. 26, 1990, 1253-1273.

[16]Cardona, A. and Geradin, M., "A Beam Finite Element Non-Linear Theory with Finite Rotations," *International Journal of Numerical Methods in Engineering*, Vol. 26, 1988, pp. 2403-2438.

[17]Iura, M. and Atluri, S. N., "Dynamic Analysis of Finitely Stretched and Rotated Three-Dimensional Space-Curved Beams," *Computers and Structures*, Vol. 29, 1988, pp. 875-889.

[18]Downer, J. D., "A Computational Procedure for the Dynamics of Flexible Beams within Multibody Systems," Ph.D. Thesis, University of Colorado, Boulder, 1990.

[19]Park, K. C., Downer, J. D., Chiou, J. C., and Farhat, C., "A Modular Multibody Analysis Capability for High-Precision, Active Control and Real-Time Applications," *International Journal for Numerical Methods in Engineering*, Vol. 32, 1991, pp. 1767-1798.

[20]Downer, J. D., Park, K. C., and Chiou, J. C., "Dynamics of Flexible Beams for Multibody Systems: A Computational Procedure," to appear in *Computer Methods for Applied Mechanics and Engineering*, 1992.

[21]Simkins, T. E., "Finite Elements for Initial Value Problems in Dynamics," *AIAA J.* Vol. 19, 1981, 1357-1362.

[22]Borri, M., Ghiringhelli, G. L., Lanz, M., Mantegazza, P., and Merlini, T., "Dynamic Response of Mechanical Systems by a Weak Hamiltonian Formulation," *Computers & Structures*, Vol. 20, 1985, pp. 495-508.

[23]Borri, M., Lanz, M., and Mantegazza, P., "Comment on 'Time Finite Element Discretization of Hamilton's Law of Varying Action'," *AIAA J.*, Vol. 23, 1985, pp. 1457-1458.

[24]Borri, M., Mello, F., and Atluri, S. N., "Variational Approaches for Dynamics and Time-Finite-Elements: Numerical Studies," *Comp. Mech.*, Vol. 7, 1990, pp. 49-76.

[25]Borri, M., Mello, F., and Atluri, S. N., "Primal and Mixed Forms of Hamiltons's Principle for Constrained Rigid Body Systems: Numerical Studies," *Comp. Mech.*, Vol. 7, 1991, pp. 205-220.

[26]Malvern, L. E., *Introduction to the Mechanics of a Continuous Medium*, Prentice-Hall, Inc., Englewood Cliffs, N.J., 1969.

[27]Vu-Quoc, L., and Simo, J. C., "Dynamics of Earth-Orbiting Flexible Satellites with Multibody Components," *J. Guidance, Control, and Dynamics*, Vol. 10, 1987, pp. 549-558.

[28]Goldstein, H., *Classical Mechanics*, 2nd ed., Addison-Wesley, 1980.